IEEE Transactions on Nuclear Science, Vol.NS-23, No.6, December 1976

SGEMP SIMULATION EXPERIMENTS WITH ELECTRON BEAMS*

R. H. Stahl, D. C. Osborn, E. P. Wenaas
JAYCOR, Del Mar, California

ABSTRACT

An alternative to utilizing laboratory photon sources, which have limited capabilities for the investigation of space-charge-limited SGEMP response, is to use large-area electron beams , which are readily available. If the experiment is analyzed by the same methods used for the analysis of a photon exposure, a validation of a major portion of the SGEMP analysis procedure is possible.

An experiment is reported in which a 30-cm diameter electron pulse from one of the Simulation Physics, Inc., generators was emitted from the center of a 60-cm diameter, 2-meter long cylinder located on the axis of a 3-meter diameter, 4-meter long vacuum tank. Magnetic field measurements were made at nine locations on the cylinder, and at the outer tank wall. The characteristics of the electron beam (peak current $\sim$3.5 kA, mean energy $\sim$12 keV, FWHM $\sim$2.5 nsec) were measured with the same diode setting and beam profile. Electron spectra were obtained with the SPI magnetic spectrometer at three radii.

Computer calculations with the ABORC code, using the measured time-dependent electron spectrum, gave excellent agreement with the magnetic fields measured at various locations on the cylinder.

INTRODUCTION

External SGEMP is concerned with the skin currents and EM fields produced at the external surfaces of an isolated object exposed to a photon pulse. The response is driven by the energetic electrons expelled from the illuminated surfaces.

Presently available laboratory photon sources do not have a photon output that is sufficiently intense to produce strongly space-charge-limited electron emission from a sizeable exposure object. To study the fields and currents that occur in such a situation, an experiment was conceived in which an electron source was located inside the object under investigation and electrons were emitted from one end of the object into a large evacuated chamber (Figure 1). The fields and currents measured from the electron-beam experiment were compared with calculations using the same methods that are applied to the analysis of photon-generated SGEMP, and thus provided a test of the analysis methods under conditions of high space-charge-limiting.

The configuration used in these measurements, therefore, differs in two fundamental aspects from the usual SGEMP problem. In the first place, only a portion of one surface of the exposure object was an electron emitter. Secondly, the exposure body was electrically connected to the tank in which the experiment took place. To determine the effect of this electrical connection, computer experiments were performed, comparing the SGEMP response in the geometry actually used with an isolated cylinder of the same diameter and half the length. The results of these calculations indicate that surface currents calculated on the cylinder that housed the electron emitter do not differ significantly from the corresponding currents calculated for an isolated cylinder for measurement locations close to the emitting surface and for times less than the clear time (the time it takes a signal to travel from the field point to the wall and back). Within these limitations, then, the geometry is a useful simulation of an isolated cylinder.

*Sponsored by the Defense Nuclear Agency under Contract DNA001-76-C-0068 with IRT Corp.

SGEMP EXPERIMENT GEOMETRY

Figure 1 shows the setup for the SGEMP experiment. The experiment was contained within a large aluminum vacuum tank, 3 meters in diameter and 3.5 meters long. An aluminum cylinder (the "shroud"), 0.6 meter in diameter and 2 meters long, electrically grounded to the vacuum tank, protruded to the center of the tank along the tank axis. Thus, the clear time for measurement positions on the front half of the shroud was greater than the electron pulse width. Electrons were emitted into the tank from the field emission diode of a Simulation Physics, Inc. SPI Pulse-6000 machine, which constituted the inner 30 cm of the 60-cm diameter front face of the shroud. The diode was connected to the voltage source by a high-voltage transmission line located inside the shroud. The cathode diameter for this application was 30 cm. Electrons emitted from the diode passed through a screen anode and a 0.1-mil Mylar window into the vacuum tank. The Mylar window is required for vacuum isolation, since the field emission diode is partially filled with gas to produce a short-duration pulse. The pressure in the 3-meter tank was less than 10^{-4} torr during the experiments.

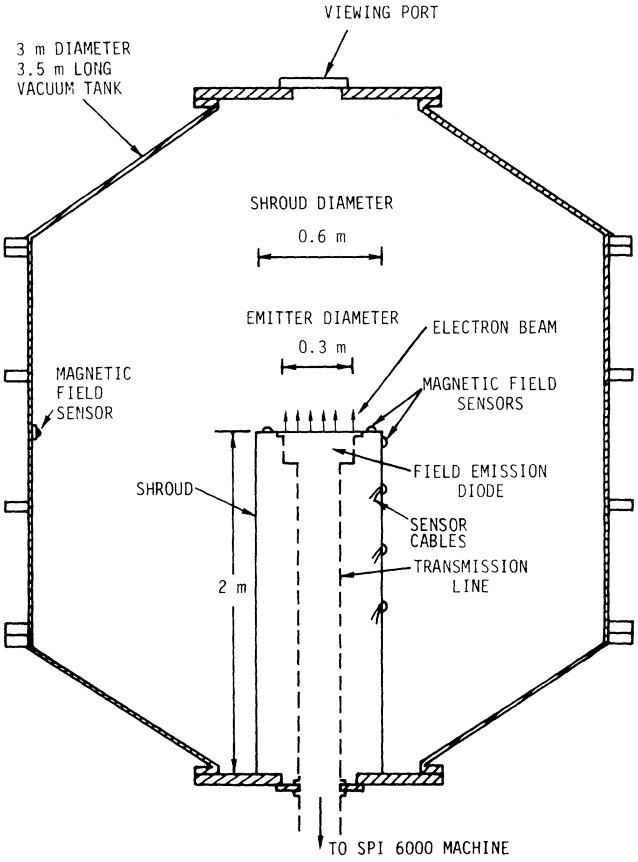

Figure 1. Experiment geometry

Figure 2 is a photograph of the shroud, showing the screen and Mylar cover over the diode and a number of magnetic field sensors. Figure 3 is a photograph giving an overall view of the inside of the tank, with a happy experimenter to indicate the scale of the hardware.

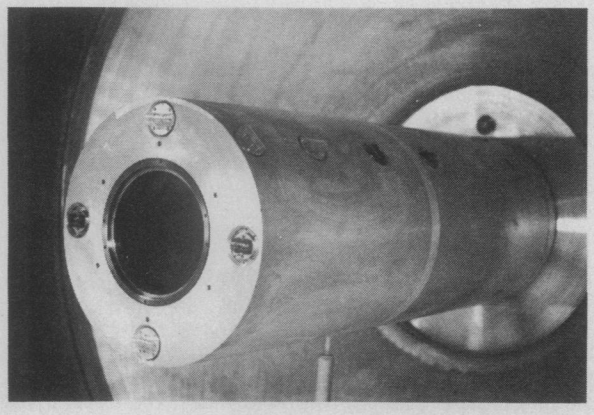

Figure 2. Photo of shroud showing magnetic field sensors and electron emitting region

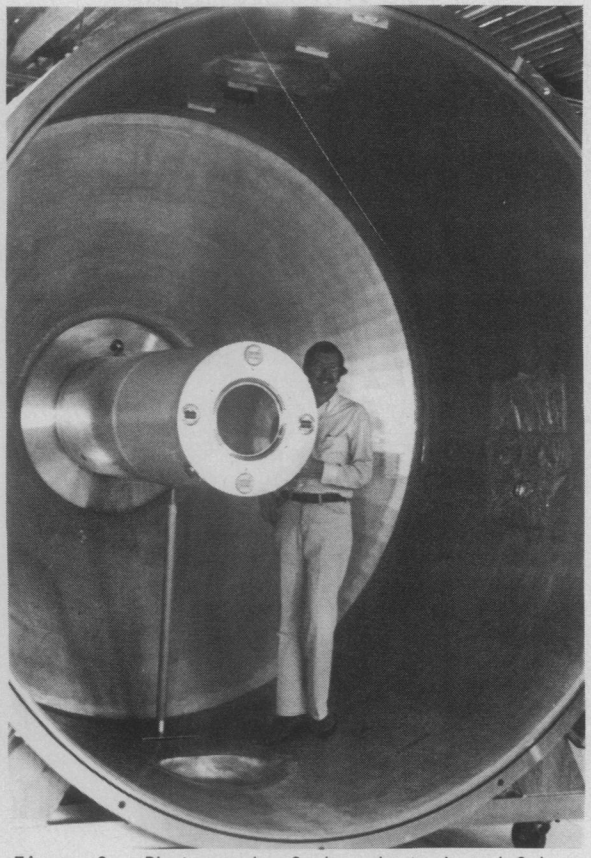

Figure 3. Photograph of shroud, tank and Osborn

Cables from the magnetic field sensors mounted on the shroud, and from the current and voltage monitors associated with the electron source, ran in the annular space between the shroud and the high-voltage transmission line to type N cable feedthroughs at the rear flange. This resulted in a remarkably clean geometry, and provided additional EM shielding for cables and connectors.

The sensors were mounted in sockets welded to the shroud; they could be rotated to place their sensitive axes parallel or perpendicular to the field expected from a symmetric electron beam out of center of the shroud.

Two types of magnetic field sensors were used in these measurements, built by EG&G, Albuquerque, to designs by Carl Baum of the Air Force Weapons Laboratory. The sensors are basically similar, differing in details of the loop construction. Both are two-turn Moebius loops mounted on a low-inductance half-cylinder to optimize the high-frequency response. The rise time of these sensors is less than 1 nsec, and the loop area 2.5 cm^2.

There were ten sensor positions on the shroud, including several redundant sets that enabled us to determine the azimuthal symmetry of the magnetic field. Four sensors were on the front face of the cylinder outside the electron beam, and two others were at the side of the shroud near the diode (one of these is obscured on Figure 2). Others extended along the 45° line of the shroud to the back wall, and an eleventh sensor was placed at the equator of the 3-meter tank outer wall.

Sensor signals were fed on balanced cables to balun transformers located outside the vacuum tank (balun rise time <0.8 nsec, attenuation factor $\sim$3.5) and recorded on Tektronix type 7904 and 7844 oscilloscopes (type 7A19 vertical amplifiers). The overall frequency response of the instrumentation could be estimated from the records of pulser measurements used to determine relative time delays in the different recording channels. For the magnetic field measurements, the rise times were about 1.0 nsec for 7904 records and 1.3 nsec for 7844 records, except for one channel which had exceptionally long sensor cables (1.5-nsec rise time). The rise time of spectrometer records was determined by the oscilloscope response.

The azimuthal magnetic field was obtained from the recorded voltage trace:

$$H(\phi)\ \text{amp/meter} = \frac{k}{n\mu_0 A}\int_0^t V_2 dt = 5.6\int_0^t V_2 dt\ ,$$

where k is the balun attenuation factor, n is the number of turns, μ_0 the free space permeability, A is the loop area, V_2 is the oscilloscope voltage, and the time integral is in V-nsec.

Figure 4 shows a typical record of a B-dot sensor; the waveforms were exceptionally clean and free from background noise. One of the test points (the top sensor on the front face) was monitored on each electron pulse; the peak value of the signal from this sensor varied by less than 10% in a sequence of 13 pulses.

BEAM CHARACTERISTICS

This portion of the work was performed jointly by the SGEMP experimenters and the wizards concerned with conjuring electrons from the SPI machine; copious experimental details are given in Reference 1.

Experience has shown that the characteristics of the pulse can be extremely sensitive to details of the diode spacing, diode planarity, and other machine adjustments which are not readily reproduced. For best results, it is essential to measure the beam parameters with the machine settings that are actually used in an experiment. Accordingly, just prior to taking the magnetic field data, SPI measured the beam profile and electron spectra.

The uniformity of the beam was measured by exposing

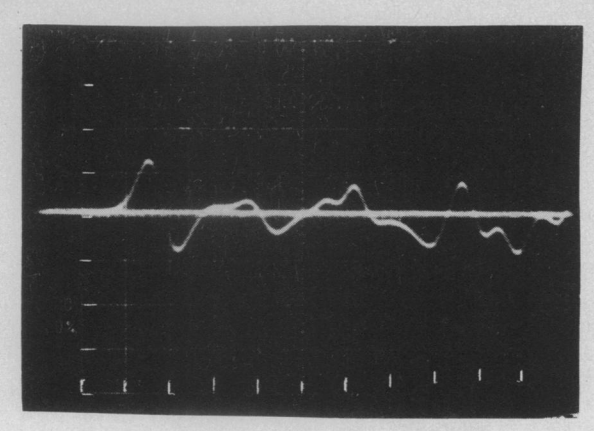

Vert: 1 V/div
Horiz: 2 nsec/div

Figure 4. Typical magnetic field measurement, B-dot sensor at outer tank wall

a 12-inch-diameter disk of x-ray film, covered with black paper and placed directly in front of the emitter in contact with the Mylar window. The film records electron bremsstrahlung from the screen and the film cover. Figure 5 is an isodensity contour map of the optical density readings from a film exposed to five sequential shots. The film measurements of the azimuthal beam variations were confirmed with an adaptation of the 4-ring Faraday cup in which all except a 60° slice was obscured, so that average current densities at various azimuthal directions could be measured.

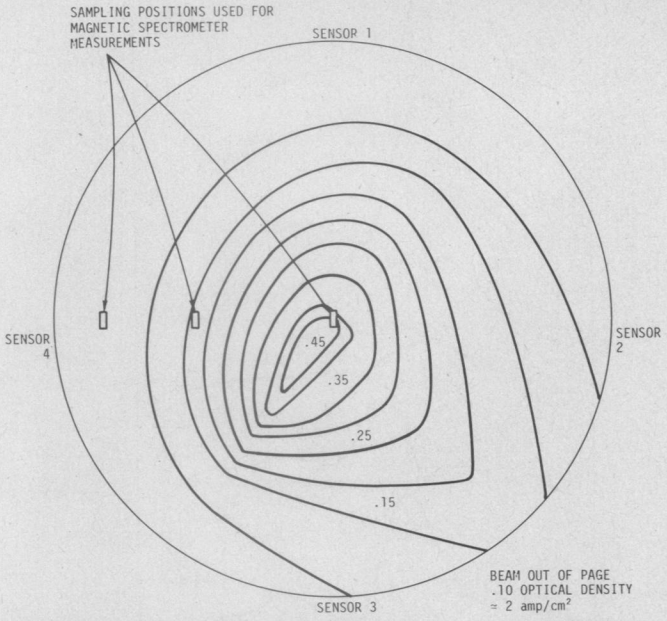

Figure 5. Isodensity map (from SPI), shots 4751-4755

The beam density is greatest near the center and falls to about one-fifth of the peak value of the outer radius. The beam is not perfectly centered and not azimuthally symmetrical; however, in the time available for the experiment, it did not appear feasible to adjust the diode for better symmetry. Previous experience in analyzing such situations had indicated that moderate deviations from ideal beam symmetry are not a serious matter as far as magnetic field measurements are concerned.

The beam was as shown on Figure 5 at the start of the magnetic field measurements. A careful examination of the sensor traces shows that the appropriate pairs (1 and 4, 2 and 3) had matching signatures that differed only slightly.

A measurement made with a 4-ring Faraday cup confirms the peaked nature of the current distribution. However, the concentric ring cup integrates over azimuthal angle and provides no precise information when the beam is not centered.

The total emitted current was measured on a single 12-inch-diameter Faraday cup. This measurement was conducted with a 12-inch-diameter chamber attached to the emitter and with the Faraday cup 0.1 cm from the Mylar window. A peak value of 3.5 kA was obtained. The total current pulse shape is shown in Figure 6. Both the pulse shape and peak amplitudes were very reproducible; during a sequence of 10 pulses, the peak amplitude varied by only 16% and the RMS deviation was 5%.

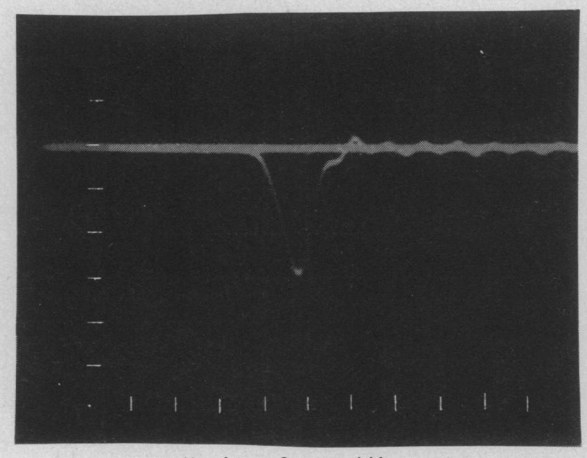

Horiz: 2 nsec/div

Figure 6. Typical electron-beam pulse; peak amplitude ~3500 amps. The oscillations at the tail end of the pulse are believed to be due to tank ringing.

Time-resolved energy spectra of the emitted electrons were obtained with SPI's magnetic spectrometer. The magnetic field was adjusted to spread the beam over 8 of the 10 collectors. Three sets of data were taken--with the entrance aperture (2 mm x 10 mm) on the axis, at a 3-inch radius, and at a 5-inch radius. There was not time to sample the beam at various azimuth angles. On these measurements, the pulse-to-pulse variation in peak current was somewhat larger than the variations in total current obtained from the 12-inch Faraday cup; the peak current on a central collector of the spectrometer varied by as much as one-third. This is consistent with the degree of fine structure of the emitted beam that is visible on the radiographs and also seen on photographs of visible light emitted from the diode region (Figure 7). The highest energy bins at the 5-inch position had larger shot-to-shot variability than the other bins: variations of more than a factor of two were seen.

Time-integrated spectra are shown on Figure 8 for the central and 5-inch-radius measurements. The data set recorded at the 3-inch radius is similar to the average of the other two. It is seen that the 5-inch position has a larger fraction of high-energy electrons, above 15 keV. The highest energy channels of the spectrometer (23 to 36 keV) had no measurable signals.

These data are the average values of a very large series of accelerator pulses--over 60 shots in all. In view of the shot-to-shot variations, it was desirable

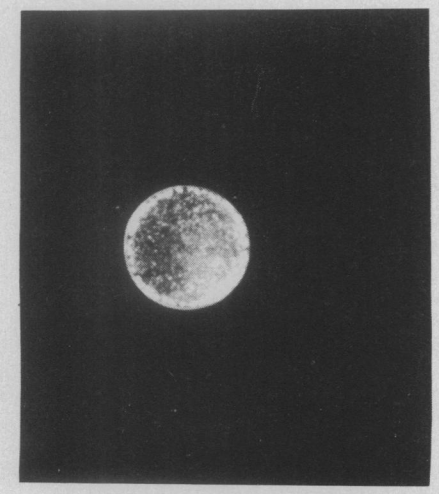

Figure 7. Open-shutter photograph of diode region, taken during pulse 4889 from the outside of the vacuum tank, showing the light from the plasma region emitted during and after the primary discharge

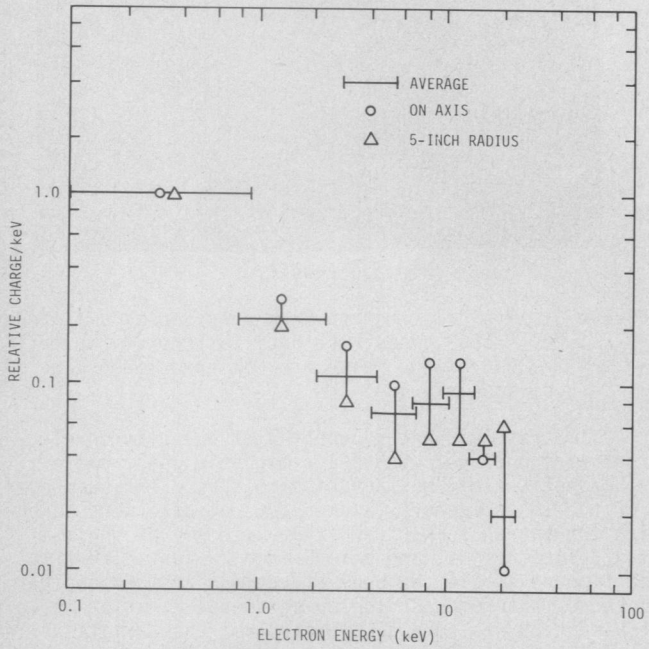

Figure 8. Comparison of time-integrated spectra

to obtain at least five data points for each energy bin at each radius, and we did not have the recording capability to record each energy bin on each shot.

On Figure 9 we show the total current waveforms, obtained by summing all the spectrometer waveforms in proper relative time, except for channel 1 (0.10-0.93 keV), which was omitted in all the calculations. The two waveforms are very similar.

Finally, on Figure 10, we reproduce SPI's reduced data from the 27 shots at r = 0. As expected, the early part of the pulse is dominated by the higher-energy electrons, and the tail consists primarily of low-energy electrons. For some reason, there is also a group of very low-energy electrons preceding the main portion of the pulse.

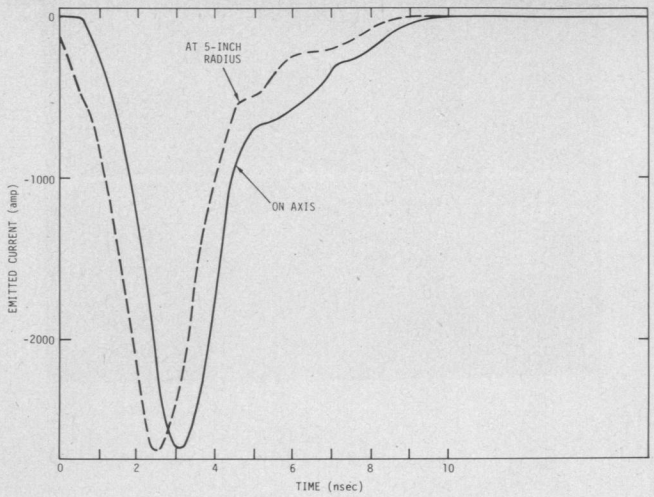

Figure 9. Comparison of emitted current waveforms determined from spectrometer measurements

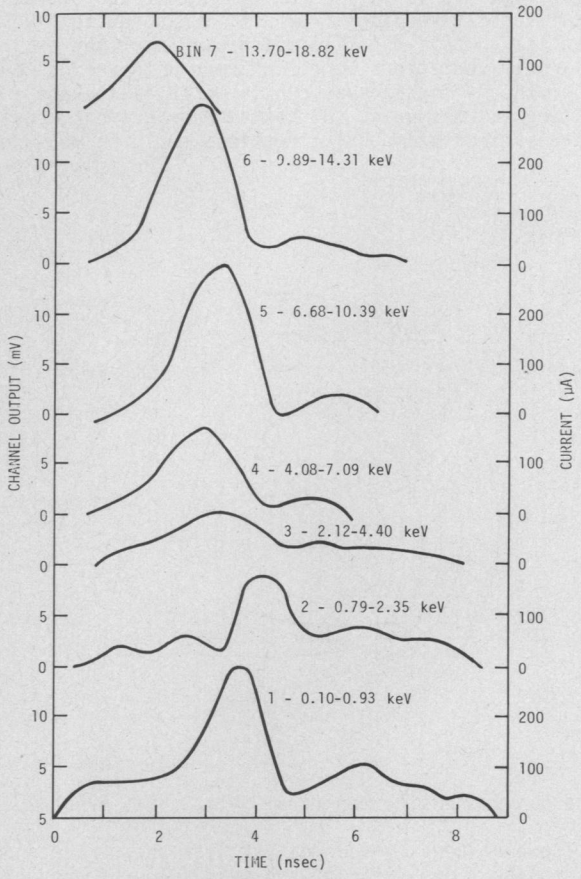

Figure 10. Time-resolved spectrometer data for SPI SGEMP experiment, SPI Pulse 6000, with diode extension; shot 4781-4807; r = 0

COMPUTER MODELING

The ABORC SGEMP code (Ref. 2) was used to calculate the response of the shroud to an electron pulse with the characteristics described in the previous section.

The ABORC code is designed to compute the SGEMP response for an arbitrary body of revolution. Electron emission may occur at any of the surfaces; arbitrary electron energy and angular distributions can be accommodated, and provision is made for time-varying electron emission. The code uses finite-difference techniques to perform a self-consistent solution of the complete set of Maxwell's equations. Variable zoning is available to permit detailed modeling of regions of special interest.

Naturally, a number of assumptions and approximations had to be made in preparing the input for the calculations:

1. The emitted current was assumed to be axially symmetric. This was a necessary assumption because ABORC cannot handle 3-dimensional complications.

2. We assumed uniform current density over the emitter area.

3. Electrons with energies below 1 keV were omitted from the calculations; they do not contribute significantly to the field.

4. Cosine-law emission of electrons was assumed, as a result of scattering in the 0.1 mil Mylar window. There is at the moment no good way to measure the electron angular distribution.

Two calculations were run with time-dependent spectra--the softer spectrum measured at the center of the diode (Figure 10) and the harder spectrum measured at the 5-inch position. For each electron bin, the appropriate measured time history was used. A third calculation, with a rather small number of particles, used the average time-integrated electron spectrum shown in Figure 8 and the same time history for all portions of the energy spectrum (the time history that is shown in Figure 9).

The following table gives some of the vital statistics for the three ABORC calculations.

	r=0 Spectrum	r=5 inches Spectrum	Integrated Spectrum
Total number of emitted particles (to 15 nsec)	10,440	13,890	3,645
Average number of active particles	1,437	2,093	615
Axial zone size at emitter	0.5 cm	0.5 cm	0.5 cm
Maximum ΔR	12 cm	12 cm	12 cm
Maximum ΔZ	30 cm	30 cm	30 cm
Zone Array: $\Delta Z \times \Delta R$	52×50	52×50	52×50
Time step-fields	10 psec	10 psec	10 psec
-particles	60 psec	60 psec	60 psec

COMPARISON OF MEASURED AND CALCULATED FIELDS

One way to compare the measured and calculated magnetic fields is to consider the amplitude of the initial peak at various locations; this has been done in Figure 11, where we give the experimental values obtained by integrating the oscilloscope records, and the calculated peak magnetic fields for the three spectra: the hard (5-inch) time-resolved spectrum, the soft (on axis) time-resolved spectrum, and the time-integrated average spectrum. It is convenient to present the field values as a function of perimetric distance from the center of the emitting surface, measured along the surface of the shroud. The solid curve is an average of the calculated peaks. We have estimated ±10% error bars for the experimented values. Note that there are four sensors at 28 cm and two at 39 cm.

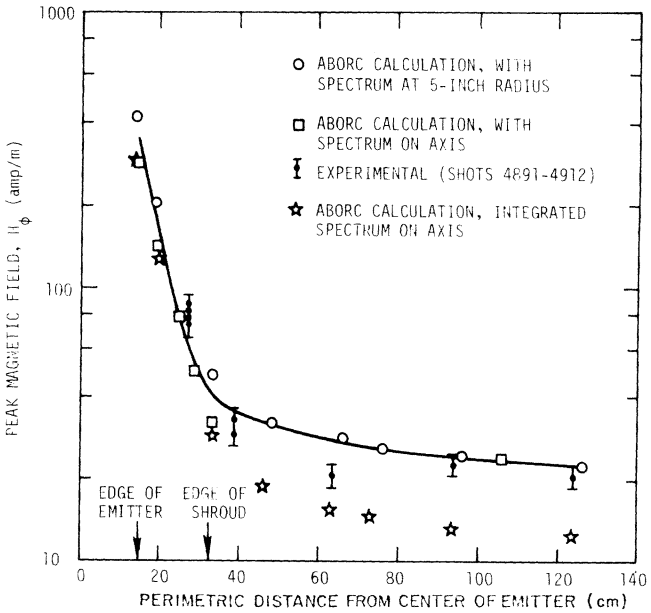

Figure 11. Comparison of measured and calculated magnetic field, first peaks

The hard-spectrum calculation produced a response 50% higher than the soft-spectrum calculation near the emitter; but at a distance of 100 cm, the responses are nearly identical. While there is a fair amount of scatter, there is reasonable agreement between these calculations and the measured results. The fields calculated for the time-integrated spectrum are systematically lower than the others, and do not agree as well with the measured values, especially at large distance from the center of the emitter.

The calculated values for the degree of limiting (defined as the ratio of the calculated field to the field that would be obtained in the absence of space-charge effects) are 0.1 and 0.15, respectively, for the soft and hard time-resolved spectra.

Another comparison of measured and calculated results can be obtained by examining the signatures obtained at several points. For this report, we will consider the sensors on the front of the shroud, and the sensor at 96 cm, near the middle of the shroud.

Figure 12 shows integrated traces from two of the four sensors at the front of the shroud (Figure 5 indicates the sensor locations). Figure 13 shows one of these, compared to the calculated value for the field at about the same location, using the r=0 electron spectrum while Figure 14 gives the calculated field for the time-averaged spectrum. In general, the agreement is rather good. The calculation with the time-dependent spectrum is rather close to the experiment, especially if one considers the smoothing caused by the limited ($\sim$ 200 MHz) frequency response of the recording system, which will erase some of the high-frequency features. The calculation with the time-averaged spectrum (Figure 14) is a

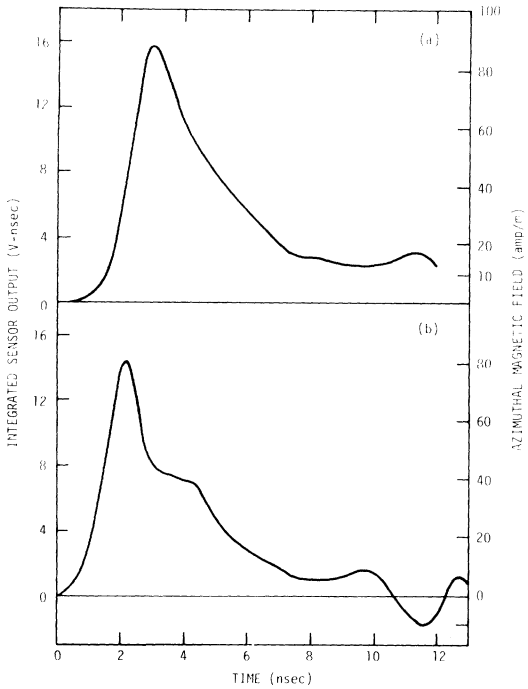

Figure 12. Magnetic field measured at 28 cm from center of emitter (a) shot 4897, sensor 2, (b) shot 4892, sensor 4 (clear time ~15 nsec)

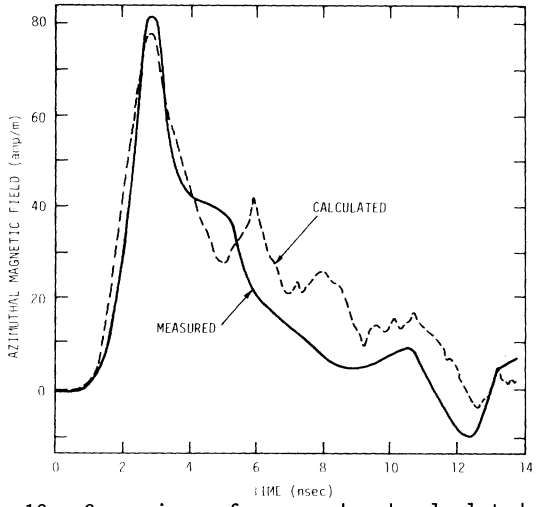

Figure 13. Comparison of measured and calculated fields at the front of the shroud, 28-cm radius (calculations with R=0 spectrum); curves normalized to time of initial peak

lot noisier than that on Figure 13 (as expected from the particle count) and shows a lot of squiggles not seen in the experiment.

Figure 15 gives a comparison of measured and calculated fields for the 94-cm position near the middle of the shroud. The degree of agreement for both the initial pulse and the wall reflections is reassuring. Even the time-averaged spectrum calculation gives a reasonable pulse shape, although the amplitude is lower.

EFFECT OF ELECTRICAL ISOLATION

Two calculations were made with ABORC to determine the effect of an electrical connection from the base of the emitting cylinder to the tank. The geometry modeled was only slightly different from the experiment. The tank was 3 meters in diameter and 2 meters long. The

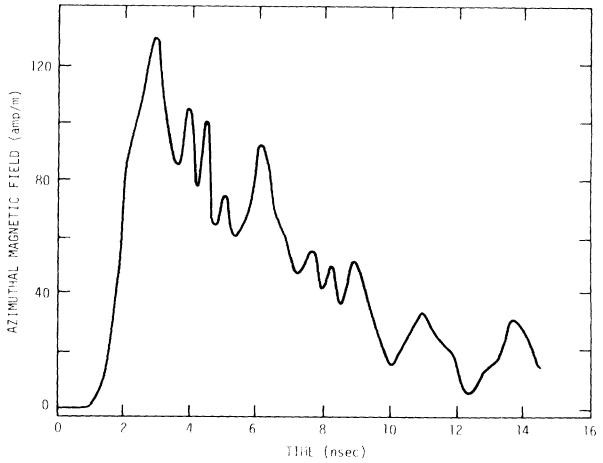

Figure 14. Calculated magnetic field at surface of shroud, 20 cm from center of emitter using the time-averaged electron spectrum

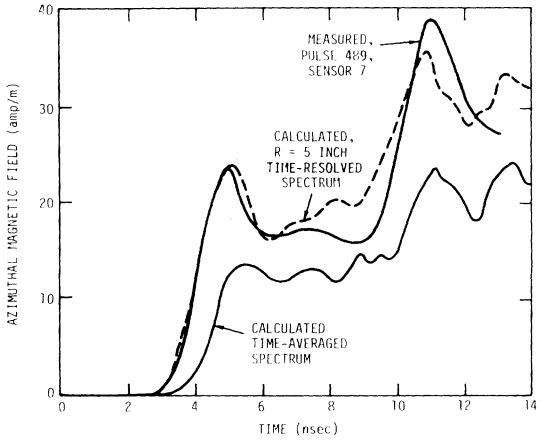

Figure 15. Comparison of measured and calculated fields near shroud midplane (94 cm from emitter center); calculations with 5-inch spectrum and with time-averaged spectrum

shroud was 1 meter long and 0.44 meter in diameter, with the correct 0.3-meter-diameter emitter. This calculation was compared to one where a 0.44-meter-diameter, 0.44-meter-long cylinder replaced the shroud, its emitting surface left in the same plane as that of the cylinder. The geometries are shown in Figure 16. The spectrum and pulse shape were somewhat different from the experimental conditions — an 8-keV blackbody spectrum and a 3-nsec triangular pulse shape.

Figure 17 compares the magnetic field time histories at a point on the side of the shroud and the cylinder, 0.14 meter from the top. The responses are identical for the first 2 nsec. The major effects of the shroud connection are a slight increase in the primary peak, and a significant increase in the secondary peak due to the reflected current from the base of the tank. The clear time (i.e., the time for an EM wave to travel to and back from the wall) in this case is about 6 nsec. Field points closer to the emitter show better agreement, while points farther away differ more radically. Thus, the shroud can be thought to approximate an isolated cylinder, at least for times less than the clear time and for field points close to the emitter.

CONCLUSIONS

1. There is good general agreement between the magnetic field measurement and ABORC calculation in a situation involving space-charge-limiting by a factor of about 10.

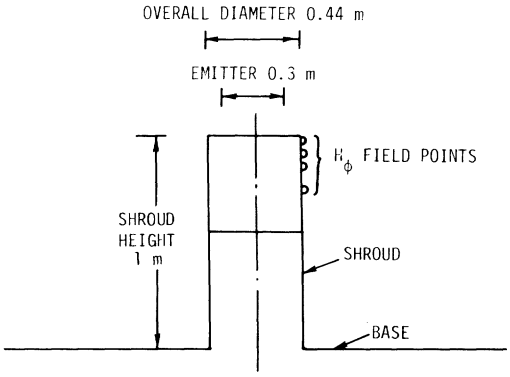

Figure 16. Comparison of shroud and cylinder geometries

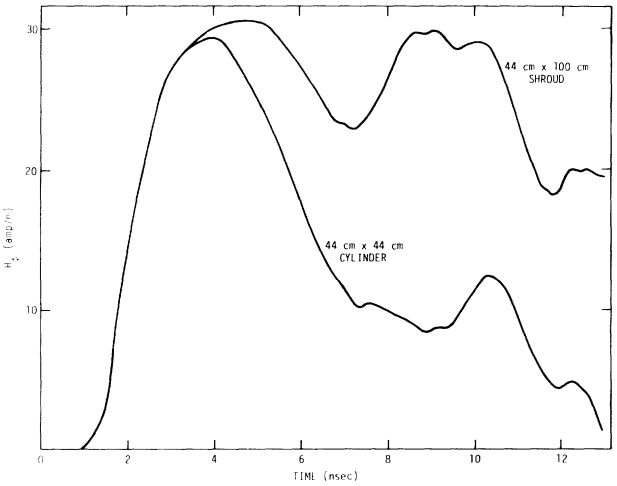

Figure 17. Comparison of shroud and cylinder responses

2. The calculations with a time-dependent electron spectrum provided a more realistic representation of the magnetic fields at the surface of the cylinder than the average electron spectrum.

3. There are several known differences between the experimental conditions and the input to the ABORC problem, principally the assumption of a flat, azimuthally symmetric current density. There are also several poorly known beam parameters, such as electron angular distribution, and variations of the electron spectrum as a function of azimuth angle. Considering factors of this type, as well as the known pulse-to-pulse variations of all the beam parameters, the degree of agreement that was found between measurement and calculation was probably as good as can be expected. It is doubtful that further measurements of surface currents in an experiment of this type can provide more critical data on the validity of the calculations. However, electric field measurements, which are much more difficult, might be considerably more useful in providing a critical assessment of the accuracy of the code calculations.

ACKNOWLEDGMENTS

This work was possible only because of the cooperation of our friends at Simulation Physics, Inc., especially R. Little and S. Face, who developed the technology for producing nanosecond large-area electron pulses, designed and built the vacuum tank and shroud, adapted the SPI Pulse 6000 to function with a 2-meter extension tube, and performed most of the work connected with beam characterization. Computer calculations were performed at IRT by A. J. Woods, T. A. Tumolillo, and S. Chaney. C. E. Mallon of IRT assisted in the experimental push, HDL lent oscilloscopes, and Raine Gilbert provided a stimulating critique of the experiment writeup.

REFERENCES

1. R. G. Little, S. H. Face, and R. A. Lowell, "The Characterization of Pulsed-Low-Voltage Electron Beams for IEMP/SGEMP Simulation," paper prepared for the 1976 IEEE Radiation Effects Conference, La Jolla, California.

2. A. J. Woods and T. N. Delmer, IRT, "The Arbitrary-Body-of-Revolution Code ABORC for SGEMP and IEMP," to be published.